THE JOURNAL OF COMPARATIVE NEUROLOGY 391:335–352 (1998)

Dendritic Properties of Hippocampal CA1 Pyramidal Neurons in the Rat: Intracellular Staining In Vivo and In Vitro

G.K. PYAPALI,[1,2] A. SIK,[3] M. PENTTONEN,[3] G. BUZSAKI,[3] AND D.A. TURNER[1,2,4]*
[1]Department of Neurosurgery, Duke University, Durham, North Carolina 27710
[2]Durham Veterans Affairs Medical Center, Durham, North Carolina 27710
[3]Center for Molecular and Behavioral Neuroscience, Rutgers,
The State University of New Jersey, Newark, New Jersey 07102
[4]Department of Neurobiology, Duke University, Durham, North Carolina 27710

ABSTRACT

Dendritic morphology and passive cable properties determine many aspects of synaptic integration in complex neurons, together with voltage-dependent membrane conductances. We investigated dendritic properties of CA1 pyramidal neurons intracellularly labeled during in vivo and in vitro physiologic recordings, by using similar intracellular staining and three-dimensional reconstruction techniques. Total dendritic length of the in vivo neurons was similar to that of the in vitro cells. After correction for shrinkage, cell extent in three-dimensional representation was not different between the two groups. Both in vivo and in vitro neurons demonstrated a variable degree of symmetry, with some neurons showing more cylindrical symmetry around the main apical axis, whereas other neurons were more elliptical, with the variation likely due to preparation and preservation conditions. Branch order analysis revealed no difference in the number of branch orders or dendritic complexity. Passive conduction of dendritic signals to the soma in these neurons shows considerable attenuation, particularly with higher frequency signals (such as synaptic potentials compared with steady-state signals), despite a relatively short electrotonic length. Essential aspects of morphometric appearance and complex dendritic integration critical to CA1 pyramidal cell functioning are preserved across neurons defined from the two different hippocampal preparations used in this study. J. Comp. Neurol. 391:335–352, 1998.

Indexing terms: CA1 pyramidal cells; neuronal reconstructions; electrotonic modeling; synaptic integration; dendritic function.

The hippocampus is frequently used as a general model of cortical development and function, but retains the advantage of a high degree of homogeneity within specific cell groups, particularly CA1 pyramidal neurons and dentate granule cells (Ramon y Cajal, 1911; Lorente de No, 1934; Minkwitz and Holz, 1975; Minkwitz, 1976; Pokorny and Yamamoto, 1981; Blackstad, 1985; Amaral et al., 1990; Lopez da Silva et al., 1990; Turner et al., 1991; Pyapali and Turner, 1994, 1996; Bannister and Larkman, 1995; Ishizuka et al., 1995). In addition, CA1 pyramidal neurons show interesting forms of dendritic properties and signal processing, including various voltage dependent properties, back-propagation of action potentials and various types of short and long-term plasticity (Christie et al., 1995; Spruston et al., 1995; Buzsaki et al., 1996; Yuste and Tank, 1996; Lipowsky et al., 1997; Magee and Johnston, 1997; Stuart et al., 1997). In contrast to dendritic homogeneity between individual CA1 pyramidal cells and dentate granule neurons (Turner and Schwartzkroin, 1980; Claiborne et al., 1992), CA3 pyramidal cells show considerable morphologic diversity depending on their location along the hilar to CA1 axis (Ishizuka et al., 1995; Turner et al., 1995).

Analyses of dendritic structure have been limited to certain techniques of visualization of neuronal morphology, including Golgi analysis or intracellular staining of

Grant sponsor: National Institutes of Health; Grant numbers: NS-29482, AG-13165, NS-27058, NS-28121, NS-02383, and 5T32 AG-00029-17; Grant sponsor: the Human Frontier Science Foundation; Grant sponsor: The Whitehall Foundation; Grant sponsor: The Veterans Affairs Medical Center.

*Correspondence to: Dennis A. Turner, M.D., Box 3807, Neurosurgery, Duke University Medical Center, Durham NC 27710.
E-mail: turne008@mc.duke.edu

Received 8 January 1997; Revised 8 August 1997; Accepted 19 September 1997

neurons by using in vitro brain slices or in vivo preparations, and in addition, various neuronal reconstruction methods have been used. Each technique of neuronal visualization involves an inherent (but often unknown) selectivity or bias of sampling from the overall population of cells. For example, some of the silver impregnation techniques (as used in the Golgi technique) can selectively identify cells in the process of dying (van den Pol and Gallyas, 1990), whereas the physiologic methods clearly require the isolation of a sufficiently healthy neuron that can withstand the rigor of sharp or patch electrode recording. In addition, slice techniques may lead to partial cell injury or loss of particular cell types, compared with in vivo visualization. Histologic techniques also show a variable amount of shrinkage due to fixation, processing, dehydration and mounting, but which may differ between various tissue planes. However, physiologic staining techniques appear to show enhanced dendritic visualization (as measured by total dendritic length) compared with Golgi analyses (Minkwitz and Holz, 1975; Minkwitz, 1976; Turner and Schwartzkroin, 1980; Amaral et al., 1990; Ishizuka et al., 1995; Turner et al., 1995). Thus, each neuronal visualization technique may introduce a particular bias in terms of both the type and extent of cells visualized.

Intracellular recordings from intact animals and in vivo labeling methods have proven invaluable to understand the axonal arborization and projections of individual neurons in the brain (Lingenhohl and Finch, 1991; Li et al., 1994; Sik et al., 1994, 1995; Buckmaster and Schwartzkroin, 1995). In the case of CA3 pyramidal neurons, a much wider range of CA3 morphologic subgroups was identified from in vivo recordings (Turner et al., 1995) than was represented in similar in vitro slice recordings (Henze et al., 1996). The present study examines the hypothesis that CA1 pyramidal neurons labeled intracellularly in vivo will demonstrate similar dendritic appearance, morphometric measurements and functional parameters compared with CA1 pyramidal neurons labeled in vitro. Convergence of dendritic properties between two different populations of similar neurons would thus suggest common, underlying principles of dendritic organization. Because different neuronal reconstruction techniques may alone lead to additional variability, we have performed similar three-dimensional reconstruction analysis for both in vitro and in vivo cells (Pyapali and Turner, 1994, 1996; Turner et al., 1995). We also present a comparative evaluation of passive signal conduction for these two groups of CA1 pyramidal neurons, which suggests similar electrotonic properties between the two different groups of neurons. A preliminary report of this work has been published (Pyapali et al., 1995).

MATERIALS AND METHODS

In vitro neuronal labeling

Two-month-old male Fischer 344 rats were killed with an overdose of halothane. This method of death was approved by the Duke University Institutional Animal Care Committee. The brain was removed and placed into cooled artificial cerebrospinal fluid (ACSF: containing [in millimolar concentration] NaCl, 124; KCl, 3.25; $NaHC0_3$, 26; NaH_2PO_4, 1.25; $MgSO_4$, 2.0; $CaCl_2$, 2.4 and glucose, 10). The hippocampi were dissected out from the whole brain and sliced in a plane transverse to the long (septotemporal) axis of the hippocampus at a thickness of 500 μm, on a manual tissue chopper (Fig. 2). Slices were maintained in ACSF for approximately 2 hours and then were placed in a surface recording chamber maintained at 36°C (Pyapali and Turner, 1994, 1996).

Bipolar, twisted-wire electrodes were used for stimulating afferent fibers in the stratum radiatum (Pyapali and Turner, 1994, 1996). Intracellular recording electrodes (1 mm thin walled capillary glass; 90 to 150 MΩ) were filled with 2% Neurobiotin (Vector Laboratory, Burlingame, CA) dissolved in 1 M potassium acetate buffer (pH 7.4). CA1 cells were impaled within the stratum pyramidale. Characteristics for a healthy impalement included a minimal resting potential of 55 mV and repetitive firing in response to intracellular depolarizing pulses. The neuronal input resistance (RN) was estimated from voltage responses after the injection of hyperpolarizing current pulses, 100-msec-long and 0.1 to 0.5 nA in amplitude. The response to orthodromic stimulation in the stratum radiatum was routinely assessed, by using a graded stimulus intensity. After this assessment, the cells were filled with Neurobiotin by using intracellular current stimulation (4 Hz depolarizing pulses, 150 msec in duration, 2–5 nA), with superimposed hyperpolarization (−0.2 nA) to prevent electrode blocking. A single cell located near the middle of the transverse slice (at a depth of 150–200 μm) was filled with Neurobiotin to increase the likelihood that all processes would lie within the slice (Pyapali and Turner, 1994, 1996).

In vivo neuronal labeling

Adult rats (2–8 months old, 200–350 grams, either sex, Sprague-Dawley strain) were anesthetized with urethane (1.3–1.5 g/kg, i.p.) and positioned in a stereotaxic apparatus. These experimental procedures were approved by the Rutgers University Institutional Animal Care Use Committee. The body temperature of the rat was kept constant by a small animal thermoregulation device. The scalp was removed, and a small (1.2 × 0.8 mm) bone window was drilled above the hippocampus (anteromedial edge at anteroposterior [AP] = −3.3 mm from bregma and lateral [L] = 2.2 mm) for intracellular recordings. The cisterna magna was opened, and the cerebrospinal fluid was drained to decrease pulsation of the brain. A pair of stimulating electrodes (100-μm each, with 0.5-mm tip separation) was inserted into the right fimbria-fornix (AP = −1.3, L = 1.0, vertical [V] = 4.1) to stimulate the commissural inputs. After the intracellular recording electrode was inserted into the brain, the bone window was covered by a mixture of paraffin and paraffin oil to prevent drying of the brain and to decrease pulsations.

Micropipettes for intracellular recordings were pulled from 2.0-mm-diameter capillary glass. They were filled with 1 M potassium acetate in 50 mM Tris buffer (pH 7.4), containing also 3% biocytin for intracellular labeling. In vivo electrode impedances varied from 60 to 100 MΩ. Once stable intracellular recordings were obtained (by using an Axoclamp-2B bridge amplifier), evoked and passive physiologic properties of the cell were determined. Next, biocytin was injected through a bridge circuit, with a 50% duty cycle of 500-msec depolarizing pulses at 0.8–2.0 nA for 5–60 minutes (Li et al., 1994). Neuronal activity was monitored throughout the procedure. Postinjection survival times ranged from 2 to 18 hours to allow complete axonal transport and staining. The degree of dendritic staining on neurons retrieved at different survival times did not vary across this time span.

Tissue processing of in vitro slices

Slices containing the Neurobiotin labeled cells were left in the recording chamber for an hour to allow active transport and diffusion of the label throughout the dendrites. The slices were then fixed overnight in 4% paraformaldehyde containing 0.1% glutaraldehyde in 0.1 M phosphate buffer saline (PBS, pH 7.4). The fixed slices were sectioned at 100 µm (nominal) on a Vibratome and collected in PBS. The 100-µm sections were found to be optimum to balance penetration of the staining reagents with a sufficiently thick section width for three-dimensional reconstructions. After three, 10 minute washes in PBS and Tris buffer (TBS, pH 8.0), the sections were incubated in 1% H_2O_2 for 30 minutes to eliminate the endogenous peroxidase activity. After the incubation, the sections were rinsed in PBS (3 times, 10 minutes), and were incubated overnight in avidin-biotin-horseradish peroxidase (HRP) complex (ABC, Vector Laboratories), diluted in 1:200 in 1% Triton X-100 dissolved in PBS. A brown reaction product was developed after incubation of the sections in 3,3'-diaminobenzidine tetrahydrochloride (DAB, 0.03% in TBS, pH 8.0) and 0.001% hydrogen peroxide (H_2O_2) containing 1% nickel ammonium sulfate for intensification. Most cells were contained within one or two sections, out of a total of four usually resulting from the sectioning. The sections were air dried, dehydrated, cleared in xylene, and cover-slipped according to a light microscopy (LM) processing and permanent mounting protocol (Pyapali and Turner, 1994, 1996).

Tissue processing after in vivo recordings

After 2–18 hour postinjection survival times, the animals were given an urethane overdose and then perfused intracardially with 100 ml physiologic saline followed by 400 ml of 4% paraformaldehyde, 0.1% glutaraldehyde, and 15% saturated picric acid dissolved in 0.1 M phosphate buffer (pH 7.3). The brains were then removed and stored in the fixative solution overnight. Sixty or 80-µm-thick coronal sections were cut on a Vibratome and processed for light microscopy in a manner similar to that used for the slices (Sik et al., 1995). In three rats, the two hemispheres were separated, and the brains were cut parallel to the long axis of the hippocampus. This different sectioning protocol placed the shrinkage into a different plane, at right angles to the coronal sections, for a comparison of the effects of shrinkage on dendritic appearance in a different direction than that observed with either coronal sections or the predominantly coronal (transverse) slices. After washing the sections for 5 minutes in 0.5% hydrogen peroxide to inactivate endogenous peroxidase, they were incubated for 4 hours in avidin-biotin-HRP complex (Vector), diluted 1:200 in 1% Triton X-100 in PBS. The peroxidase reaction was developed with nickel-ammonium sulfate-intensified 3,3'-diaminobenzidine (DAB-Ni) as a chromogen, to produce a deep blue to black endproduct (Sik et al., 1995). The sections were air dried, dehydrated, cleared in xylene, and cover-slipped.

As discussed below, the sections processed using the light microscopic protocol experienced considerable shrinkage in the slice or section depth, due in large part to dehydration. To reduce this shrinkage and as alternative method to view dendritic structure, brain sections from five rats were processed according to a electron microscopic protocol (EM). Sections were washed several times in 0.1 M PBS, immersed in cryoprotective solution (25% sucrose, 10% glycerol in 0.01 M PBS), freeze-thawed in liquid nitrogen, and washed again in several changes of 0.1 M PBS, before being incubated in ABC solution (2 hours to overnight). They were treated with 1% OsO_4 for 1 hour, dehydrated in ethanol and propylene oxide, counterstained with uranyl-acetate, and embedded in Durcupan (Sik et al., 1995). The cryoprotective solution, osmification, and lack of air drying prevented much of the shrinkage in the depth of the section, as discussed below.

Shrinkage correction of neurons labeled in vitro

Cells that were incomplete, showed a weak peroxidase reaction or demonstrated clearly truncated dendritic branches were excluded, usually due to the obvious loss of a critical section with the processing. Shrinkage was estimated by microscopic measurements of the overall slice dimensions ($n = 5$) along the axis parallel to the pyramidal cell layer (X axis in Fig. 2) and the axis perpendicular to the pyramidal cell layer (from the alveus to the hippocampal fissure - Y axis in Fig. 2) while still in the chamber and then after fixation and dehydration. Another set of measurements ($n = 5$) were performed on sections cut at a nominal thickness of 100 µm from the midpoint of the hippocampus. These sections were measured after fixation by mounting the sections in phosphate buffer under a coverslip and using a ×40 oil immersion lens, then measuring the perimeter and area using Neurolucida. The section thickness (in the septotemporal direction or at right angles to the long axis of the hippocampus - Z axis in Fig. 2) was noted before processing for each slice individually, by measuring the depth of the tissue sections after mounting under the coverslip. The depth was measured using the micrometer on the microscope (calibrated in micrometers) and carefully noting the edges of the tissue in at least four locations for each slice, before dehydration and processing.

After air drying, dehydration, and processing, the perimeter, area, and depth were again measured in a similar manner for each slice, using Neurolucida and the ×40 oil immersion lens with a coverslip. Ten to eleven percent shrinkage was observed in each of the X and Y planes due to the dehydration step, according to both linear and areal measurements comparing each individual slice before and after the processing. There was also considerable shrinkage in the Z plane due primarily to air drying and dehydration after mounting, averaging 25–27% residual tissue depth (for example, in the Z plane, a 100-µm-thick section averaged 25–27 µm after fixation and dehydration). The correction factors for this shrinkage were defined to be 1.13 in each of the X and Y planes and 4.0 in the Z plane (or a simple average of 2.09 across all planes). The morphometric measurements (including both dendritic diameter and length) and reconstructed views were corrected in each plane individually for this estimated shrinkage (Pyapali and Turner, 1996). Note that any shrinkage of the slice during initial processing, before and during physiologic assessment in the recording chamber, and with fixation was not measured with this technique.

Shrinkage correction of neurons labeled in vivo

To assess the degree of shrinkage, four penetrations into the brain were made by a 100-µm-diameter tungsten

microelectrode (2 × 2 mm distance apart in lateral and anteroposterior directions), by using stereotaxic coordinates. The rat was then perfused, and the sections were treated as described above. The middle of the tracks at the same depth in the hippocampus was determined and the distances were measured. Before histologic processing, the brain shrank 10 and 15% in the depth of the section and across the plane of the section, respectively. After histologic processing a further 10% shrinkage was observed in the plane of the section giving a total of 25% linear shrinkage in this plane. In the longitudinal direction, the total shrinkage could not be determined, because this latter procedure was carried out on the already sectioned brain tissue. However, when the thickness of the sections were determined by focusing the top and the bottom surfaces of the sections in the microscope, an approximately 75% total shrinkage was calculated in the depth of the section, similar to that observed for the in vitro slices. In addition, in several instances, distances between identified marks (e.g., vessels) were determined in wet sections immediately after cutting the brain and again after histologic processing. These measurements were carried out on sections before and after processing, using sections in both cases mounted on slides under coverslips and assessed using an oil immersion lens, and the depth was measured using the microscope focusing micrometer.

Using the light microscopy processing protocol, a 25% shrinkage was measured in both of the directions of the plane of the coronal sections, and 75% shrinkage in the depth direction, perpendicular to the coronal and longitudinal sections. These values for shrinkage was confirmed using three separate sets of sections. Note that this shrinkage for the in vivo cells is slightly more than with the in vitro cells despite a similar processing protocol because shrinkage after removal from the brain is also included in addition to the shrinkage resulting from fixation and processing. The correction factors applied to all dimensions for cells visualized using this processing were 1.33 in the plane of the section (transverse for coronal sections) and 4.0 in the depth direction (thickness of the section; average of 2.22).

However, for the sections prepared with the electron microscopy protocol, we estimated the shrinkage for sections to be symmetrical and 20% in each of the axes; a correction factor of 1.25 was applied to all three dimensions for these cells (average of 1.25). This shrinkage was also measured on the same sections mounted before and after the processing under coverslips and with an oil immersion lens, We purposely changed the orientation of the tissue sectioning and the method of fixation and processing to firmly establish the actual three-dimensional structure of the CA1 cells. Overall, three different factors were used for shrinkage correction, depending on the processing conditions used for each single cell: (1) in vitro light microscopy, (2) in vivo light microscopy, and (3) in vivo electron microscopy processing.

Selection and reconstruction of the labeled neurons

Complete and optimally labeled CA1 hippocampal pyramidal cells fulfilled the initial requirement that cells should extend from the alveus to the hippocampal fissure. These cells were densely labeled so that all visible processes, including dendritic spines, could be followed at high magnification (Fig. 1). Only a single cell was filled in a hemisphere or a slice. Neuronal processes were reconstructed across all sections containing processes by using a ×100 oil immersion lens (N.A. = 1.25) and a computer-based neuronal reconstruction system which included an automated stage and high-resolution monitor viewed through the microscope drawing tube (Neurolucida; Microbrightfield, Colchester, VT). This system allowed accurate tracing of the cell processes in all three dimensions while allowing frequent verification and recording of dendritic diameters by using a circular cursor. Each field of processes was traced with a bitpad cursor while viewing the cell and the computer monitor simultaneously, and branches were followed sequentially, one microscope field at a time. Focusing to maintain processes in clear view was performed via a joystick controller, and these changes in the depth axis were continuously recorded by the computer program, together with the X-Y in the plane of the section or slice. Dendritic branches that continued into the next section were marked as "incomplete endings." The adjacent section was then superimposed over the computer overlay viewed on the monitor (the tracing of the previous section), and the incomplete dendritic branches were aligned with appropriate processes in this new section, and the tracing was continued. The fully digitized representation of the neuron in three dimensions could be viewed or edited to ensure accuracy compared with the original cell.

Each neuron consisted of approximately 10,000–25,000 digitized data points (depending on the size of the cell), encoding the X, Y, Z coordinates for each data point with their respective dendritic diameters and the vector endpoints for each dendritic branch. The digitized neurons were viewed on the computer, rotated in three dimensions to obtain desired views, and then any particular position could be printed as a two-dimensional view. These data lists were simplified for the electrotonic analysis to a cable format by eliminating the three-dimensional structure and contracting branches with a constant diameter together between branch points; this reduced structure contains branch segments that consolidate many of the original branches (Turner, 1984a; Turner et al., 1991; Table 1). Morphometric analysis (summed geometric path length and branch order analysis; Uylings et al., 1986; Bannister and Larkman, 1995) was also performed. The shrinkage described above was corrected in three separate dimensions on the neuronal views and the morphometric data. However, because the three-dimensional structure was purposely not maintained for the electrotonic analysis then the appropriate, single averaged shrinkage value was used only in this particular type of analysis.

Summed path length and branch order analysis

The summed path length to all terminating branches from the soma was calculated initially by using geometric length and then plotted as a histogram. Additionally, the number of dendritic branches at each branch order and average dendritic branch length per branch order were plotted against branch order number. Branch order incremented at each branch point in a centrifugal fashion, starting at 1 for branches connected to the soma. Maximum branch order represented the total number of branch points between the soma and the most terminal branch segment.

Electrotonic modeling

Cells were briefly evaluated for synaptic efficacy by using a passive cable model (Turner, 1984a, 1984b). Basic

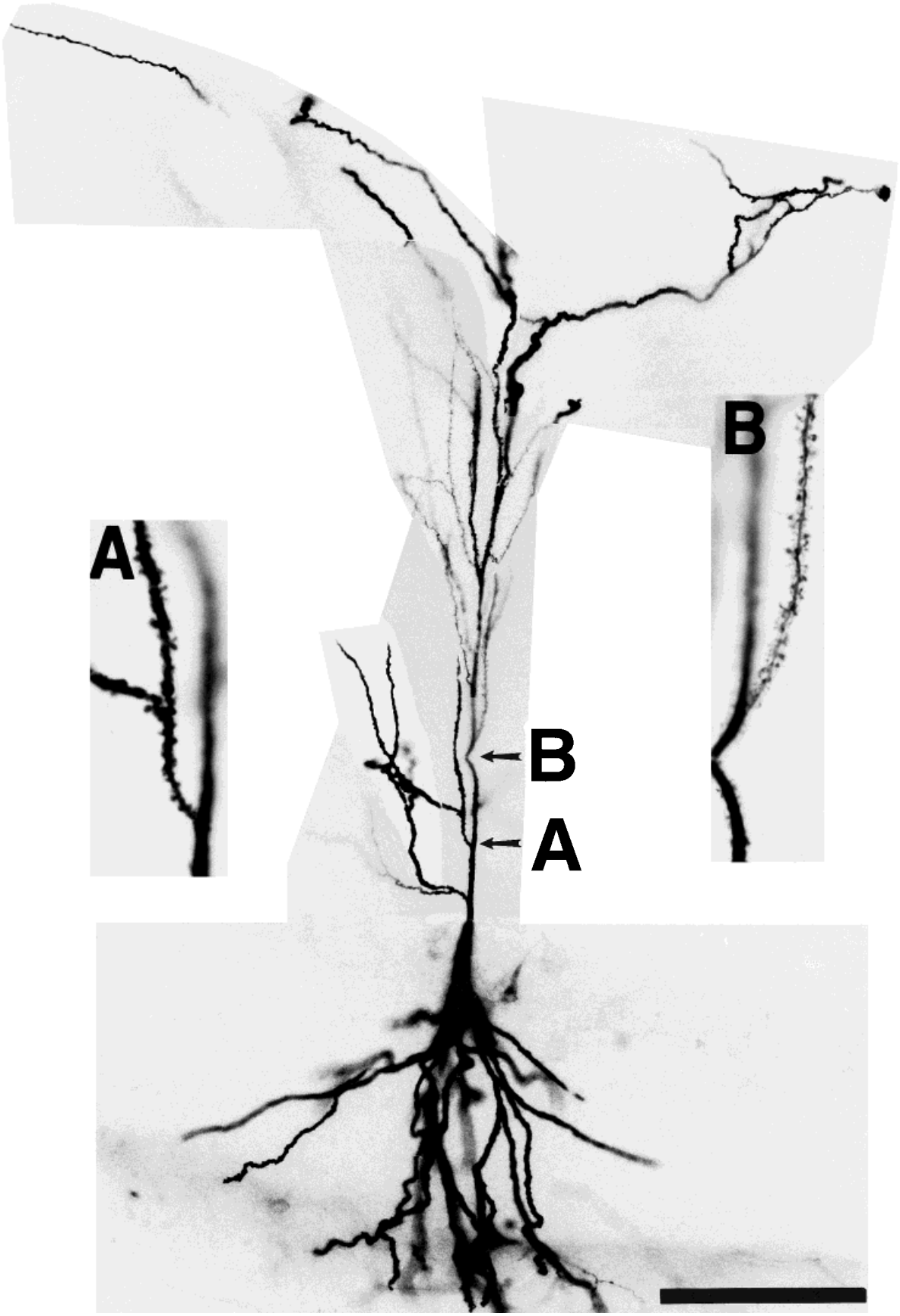

Fig. 1. CA1 pyramidal cell labeled with biocytin, shown as a collage from photomicrographs taken at several depths of focus. The inset areas indicated by arrows (arrows, **A,B**) are shown at 5× larger magnification in the insets. Note the difference in the diameters of the two main apical branches and the profuse number of small dendritic spines. Scale bar = 100 µm in main figure, 20 µm in insets.

TABLE 1. Morphometric Data—In Vitro and In Vivo[1]

Parameter	In Vitro Cells (n = 11)	In Vivo Cells (n = 23)	*P* Value
Length			
Total dendritic length (mm)	16.3 ± 4.33	17.4 ± 3.90	NS
Apical dendritic length (mm)	11.3 ± 4.08	10.6 ± 2.45	NS
Basilar dendritic length (mm)	5.07 ± 1.16	6.89 ± 2.11	*
Volume extent			
X-axis extent (μm)	247 ± 34.3	274 ± 58.3	NS
Y-axis extent (μm)	701 ± 95.6	697 ± 102	NS
Z-axis extent (μm)	202 ± 73.6	170 ± 94.1	NS
X|Z ratio	1.42 ± 0.64	2.04 ± 0.88	*
Apical tree			
Total number of main trees	1.55 ± 1.21	1.10 ± 0.31	NS
Number of branches	62.2 ± 22.4	50.1 ± 14.7	NS
Number of endings	63.8 ± 22.3	38.0 ± 26.1	NS
Number of oblique branches (SR)	19.0 ± 5.64	17.9 ± 5.10	NS
Number of apical tuft branches	7.00 ± 2.61	6.10 ± 3.06	NS
Maximum branch order	22.2 ± 3.82	21.5 ± 4.02	NS
Basilar tree			
Total number of main trees	4.64 ± 0.92	3.85 ± 0.98	*
Number of branches	23.9 ± 8.06	30.2 ± 9.13	NS
Number of endings	28.8 ± 8.17	34.0 ± 9.59	NS
Maximum branch order	6.82 ± 1.40	7.50 ± 1.73	NS
Branch data			
Maximum branch orders	23.3 ± 5.10	22.1 ± 5.37	NS
Number of branch points	85.4 ± 24.3	80.2 ± 17.8	NS
Number of segments	202 ± 54.3	200 ± 58.4	NS
Number of terminals	91.3 ± 24.1	84.6 ± 18.8	NS
$d_{3/2}$	1.70 ± 0.09	1.64 ± 0.14	NS

[1]Values are mean ± SD. The number of apical and basilar trees indicates the main stems arising from the soma. The total number of branches represents sum of all the branches in the tree. SR, stratum radiatum; apical tuft, the distal part of the apical tree in stratum lacunosum-molecular. $d_{3/2}$ represents a comparison of branching between parent and daughter branches (see text). NS implies that $P > 0.05$, or not significant; asterisk implies $P < 0.05$ (see text for a description of the statistical tests).

parameters were assumed to lie in a "reasonable" range, and the use of different parameter values may alter slightly many of these derived parameters (such as electrotonic length: Claiborne et al., 1992; Spruston et al., 1993, 1994; Stockley et al., 1993; Major et al., 1994; Migliore et al., 1995; Henze et al., 1996; Mainen et al., 1996). The cells were modeled by using a presumed specific membrane resistance value of 30 KΩ-cm^2 (Spruston and Johnston, 1992), a specific internal resistivity value of Ri = 200Ω-cm, a "sealed-end" termination for terminal segments and a linear (averaged) shrinkage correction factor as discussed above. Specific membrane capacitance was assumed to be 1.0 μF/cm^2 so that the assumed membrane time constant was 30 msec. The measured neuronal input resistances were not specifically used for this analysis, because it was assumed that a considerable somatic "leak" was present due to the sharp electrodes. Dendritic spines were included, but from a "standard" distribution (derived from Golgi studies and shown explicitly as a function in Turner [1984a]) and density (peak at 1.8 spines/μm: Turner, 1984a; Trommald et al., 1995), because neither the distribution nor density were measured from these neurons. This standard distribution includes a function describing a variable spine density depending on the geometric distance from the soma, as has been measured for several classes of Golgi cells, but with the maximum value estimated from recent Lucifer yellow stained neurons (Trommald et al., 1995). Additionally the electrotonic distance or summed electrical path length from the soma to all dendritic terminals was calculated given these assumptions, and histograms of the distribution of values were plotted.

Voltage transfer from a dendritic site (spine or shaft) to the soma and from the soma back to the same dendritic site were separately calculated by using a passive cable format that defined both a frequency domain filter and a time-domain transfer function for convolution with any input function (Turner, 1984b). These filters were specific to each site and to the direction of input due to the difference in the terminating impedances between the two directions of signal propagation. Specifically two separate inputs were considered, originating either at the soma and measured at various dendritic regions or originating at dendritic sites and measured at the soma. These two passive inputs were a steady-state constant input and a typical waveform shape for a fast (such as a non-*N*-methyl-D-aspartate [NMDA] response) synaptic input (fast excitatory postsynaptic potential [fEPSP]; $\alpha = 20$; time to peak of 1/20 α, or ~1.5 msec, with a normalized α function; Turner, 1984b). To average across neurons, 24 dendritic sites were selected at random from each cell, and the transfer ratios for these sites (for the two signals and in each direction) were then plotted as graphs of voltage transfer vs. electrotonic length.

Statistical comparisons

The grouped data were compared with analysis of variance and where appropriate, individual unpaired t tests. The significance is given as either $P < 0.05$ (*), $P < 0.01$ (**), or $P < 0.001$ (***) in the tables and graphs.

RESULTS

Neuronal morphology

The populations of cells recorded and adequately visualized from normal animals include 11 CA1 neurons stained in vitro and 23 CA1 cells labeled in vivo, all reconstructed in a similar fashion using the Neurolucida setup. Intracellular iontophoresis of the dye for 10–30 minutes resulted in excellent, uniform labeling of the cells (Fig. 1). The overall dendritic appearance was similar in all neurons labeled both in vitro and in vivo, including a basilar bush extending from the cell body or pyramidal layer to the alveus, usually a single apical dendritic tree with proximal side branches within the stratum radiatum, a few large branches penetrating the stratum radiatum/stratum lacunosum-moleculare border, distinct lateral dendritic branches in the lacunosum-moleculare and extension of the neuron from the alveus to the hippocampal fissure (Fig. 1). The cells possessed a thick covering of small dendritic spines (views in Fig. 1 A,B).

We altered both the orientation of tissue sectioning (coronal or longitudinal) and the method of fixation and processing (LM or EM) in subgroups of cells to infer the actual three-dimensional structure separate from shrinkage artifacts. Figure 2 schematically shows the position of these CA1 pyramidal cells within the three-dimensional matrix of the hippocampus (either a histologic section or a slice) and the labeling of the three axes and planes in which they are oriented. A fully cylindrical neuron gives a symmetrical view along the X Z axis, as shown in this example through the alveus and from the ventricular surface. An important question to be addressed by the data is whether there is a particular three-dimensional structure of the cells in relation to the overall hippocampus, as, for example, can be observed with the orientation of Purkinje cells along the direction of cerebellar folia.

Quantitative analysis of dendrites

The total dendritic length (TDL) of labeled in vivo CA1 neurons was similar to that of the in vitro CA1 cells, as

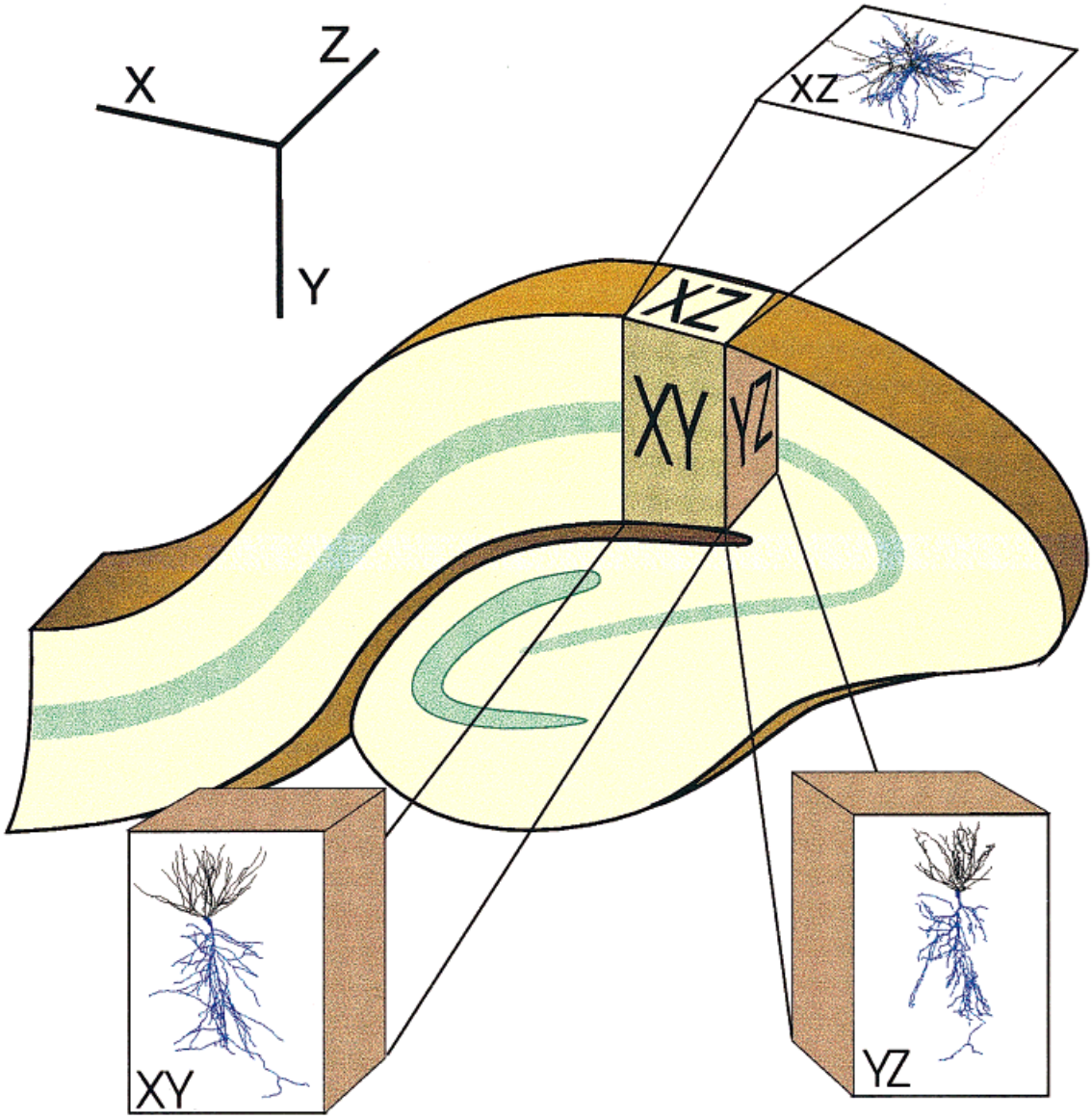

Fig. 2. Diagrammatic representation of either a transverse hippocampal slice or a section from an intact hippocampus, showing the three-dimensional position of a CA1 pyramidal neuron within the anatomical boundaries of the hippocampus. The XY, YZ, and XZ orientations of the cell are shown in the faces of the cubes.

shown in Table 1. However, the total basilar dendritic length was longer for the in vivo neurons. The extent of these cells along the long axis (Y; perpendicular to the pyramidal cell layer, between the alveus and hippocampal fissure) was equivalent, as was the extent across the radiatum in the transverse plane (X; parallel to the pyramidal cell layer; Table 1). After appropriate correction for shrinkage, the septotemporal extent (Z) was also similar between the groups (Table 1). This similarity implies that after correction for the variable shrinkage in the three dimensions there is a elliptical or cylindrical symmetry between the dendrites extending along the X dimension and the Z dimension, as would be viewed from the X Z plane, equivalent to looking down at the neuron from the ventricular surface (Fig. 2).

Based on the relative X Z ratio (Fig. 2) the in vivo CA1 pyramidal cells were initially divided into two subgroups: those with elliptical profiles (X Z ratio > 1.5, 61%, $n = 14$) or those that exhibited roughly cylindrical profiles (X Z ratio < 1.5, 39%, $n = 9$, Fig. 3). Representative cells are shown in Figure 3 and their dendrograms in Figure 7. These figures also show the correction for shrinkage, as described in Methods, with differential shrinkage values applied for the three planes as measured. Figure 4 shows a summary of the X Z ratio, with a large overlap between the in vivo and in vitro groups. There was no difference in the number of branches or endings in both the apical and basilar trees between the two groups (Table 1). However, there was a significant difference in the number of basilar trees arising from the soma. The contribution of basilar

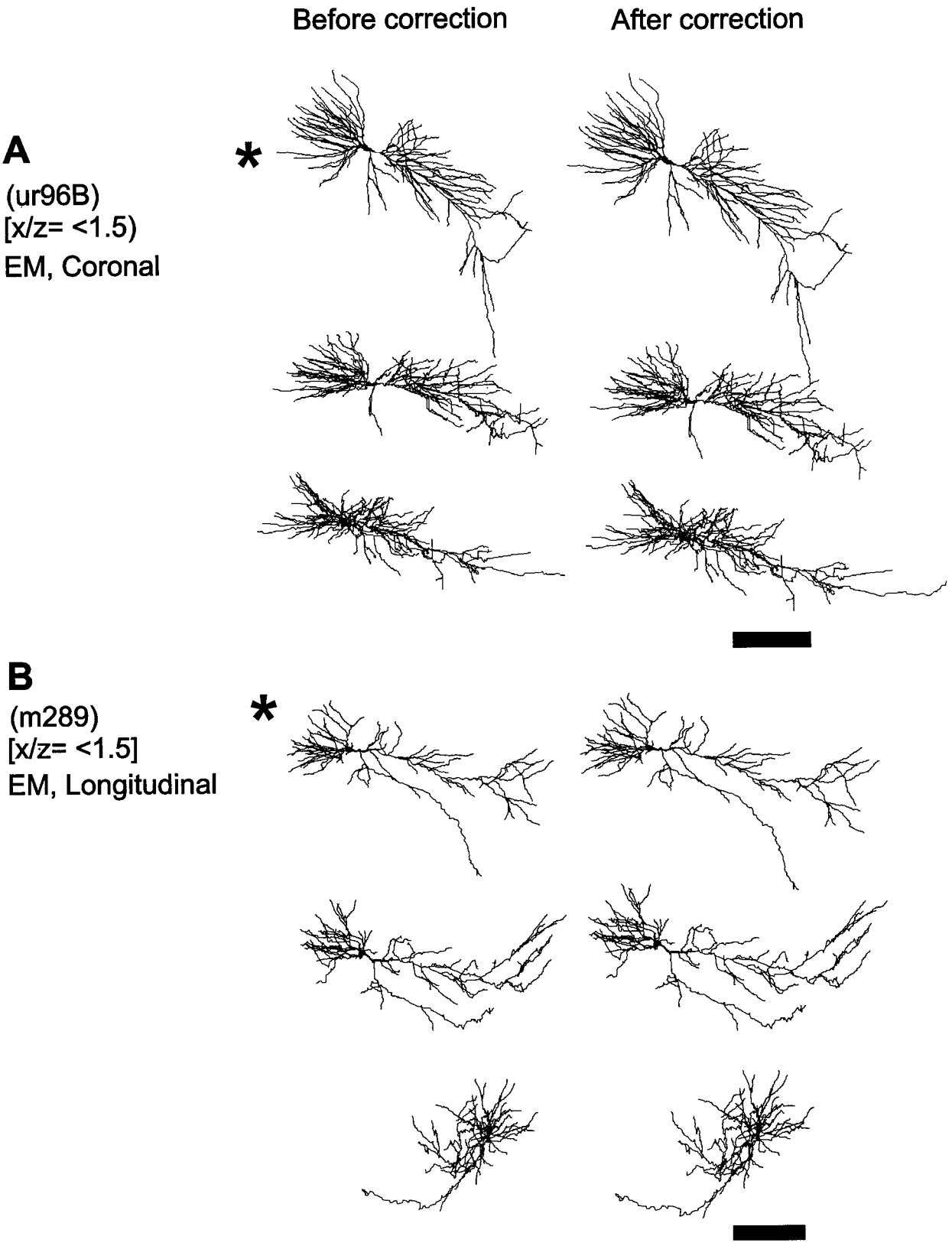

Fig. 3. Representative examples of reconstructed cells. The XY, YZ, and XZ representations (as shown in Fig. 2) before and after correcting for shrinkage in all the three directions are shown. Asterisks indicate the primary view in which the cell was reconstructed. **A:** Cell was cut coronally or transversely along the hippocampal axis and processed for electron microscopic (EM) visualization. **B:** Cell was cut parallel to the long hippocampal axis (longitudinal) and was processed for EM visualization. The XY, YZ, and XZ representations (as indicated in Fig. 2) are shown before and after correction for shrinkage in all the three directions. The primary view in longitudinally cut cells is the Y-Z view (see Fig 2). Processing the cell for light microscopic visualization resulted in significant amount of shrinkage in the Z-axis, whereas processing for EM resulted in minimal and symmetrical degree of shrinkage in all three directions. Note that both cells are fully cylindrical upon correction for shrinkage. **C,D:** A typical slice cell (C, in vivo and D, in vitro), cut from coronal sections and processed for light microscopy, which on correction for shrinkage were fully cylindrical. Scale bars = 200 µm.

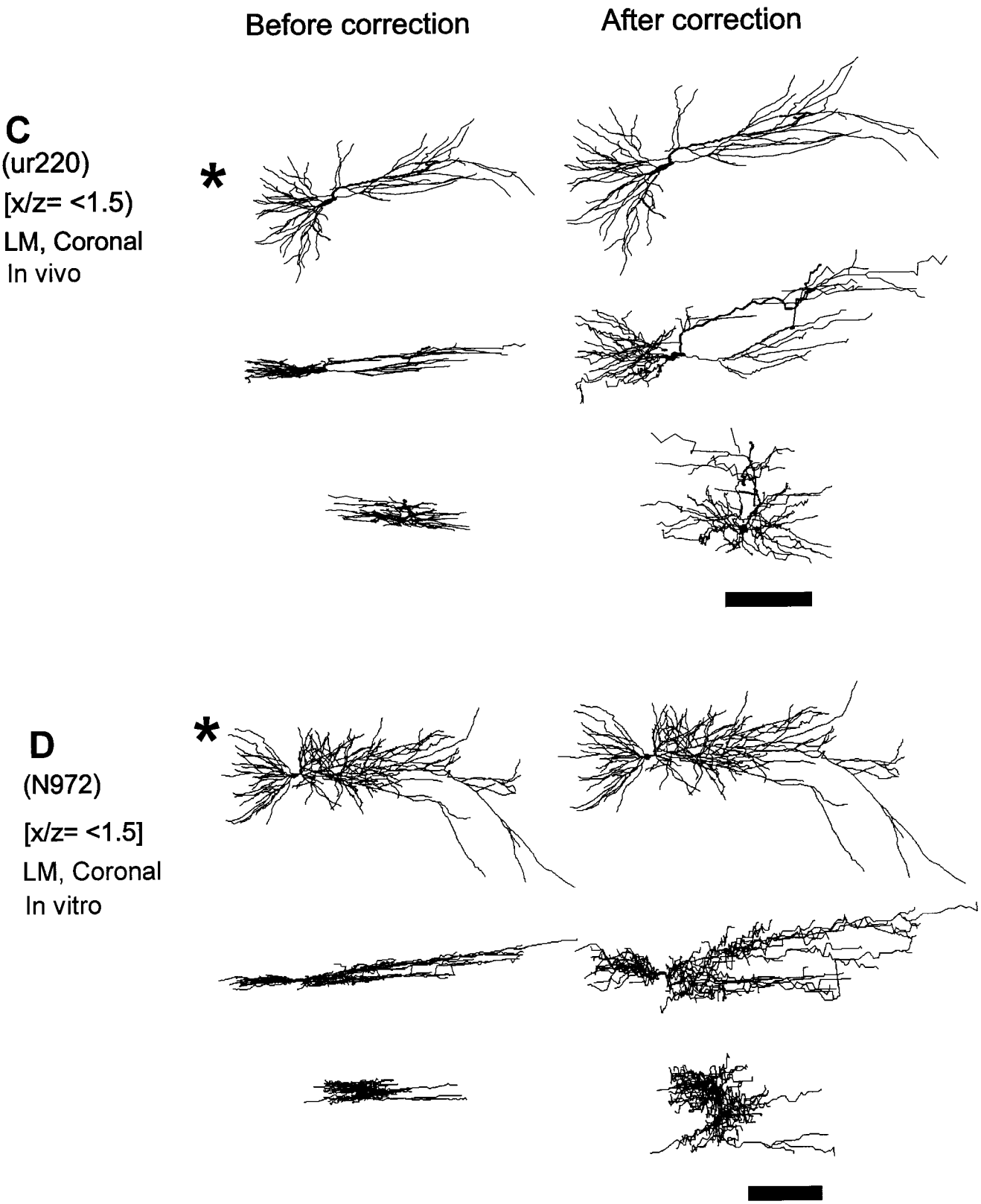

Figure 3 (Continued)

trees to the total dendritic length was slightly higher in the in vivo cells (BDL = 39%, ADL = 61%) compared with the in vitro cells (BDL = 31%, ADL = 69%). Note that a large shrinkage in the depth axis can lead to an artifactually flatter appearing neuron in this axis, indicating that determination of the degree of shrinkage is a critical step

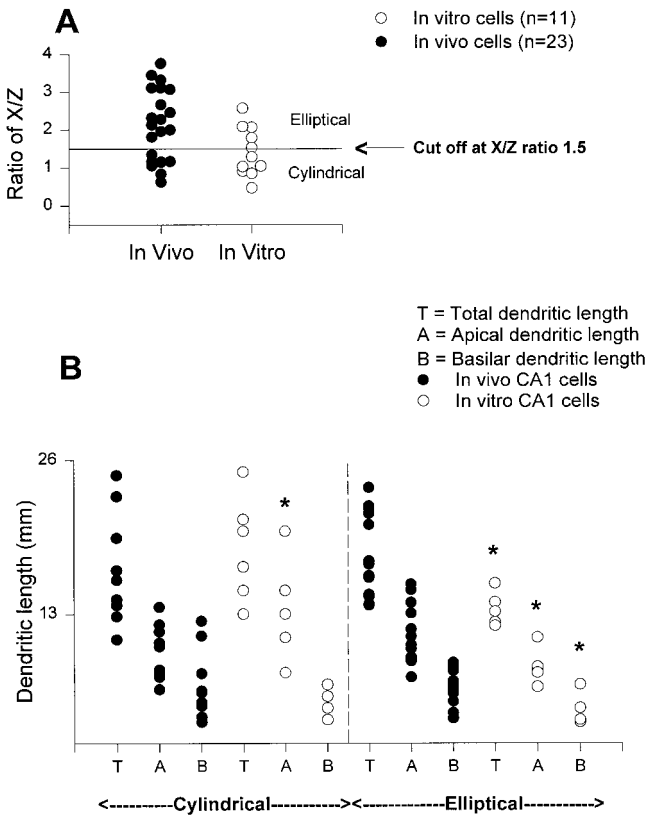

Fig. 4. **A:** X-Z ratios of in vitro and in vivo filled cells. The CA1 pyramidal cells were separated into cylindrical (cut off <1.5) and elliptical (cut off >1.5) types from their three-dimensional appearance. **B:** Total, apical and basilar dendritic lengths of in vivo and in vitro CA1 pyramidal cells. Asterisks indicate significant difference between the in vivo and in vitro cell types.

in determining whether other factors are also involved in the differences between the in vivo and in vitro cells (Fig. 3C,D).

We included two sets of control conditions for the in vivo neurons to assess whether all neurons in vivo are cylindrical. The first condition was longitudinal sectioning, in which the largest plane of shrinkage proved to be tissue depth, now oriented to the mediolateral axis rather than the septotemporal axis (n = 3 cells). With this type of sectioning the elliptical shape was transferred to the Y rather than the X axis, suggesting that inadequate compensation for shrinkage was the main reason to obtain the elliptical shape. An additional control was to change the embedding procedure after sections were cut, to an EM embedding procedure in a much harder media (n = 5 cells). This type of embedding led to a decreased shrinkage in all planes and all cells embedded with the technique showed a cylindrical appearance on reconstructions (Fig. 3B). Thus, adequate correction or control of shrinkage altered the three-dimensional appearance of both the in vivo and in vitro neurons to give a more cylindrical profile. However, there is no equivalent control currently for tissue changes secondary to the slicing procedure or the bath and recording conditions prior to which shrinkage can be initially measured, for the in vitro neurons. However, after correction for the identified shrinkage the in vitro neurons were predominantly cylindrical (Fig. 4), suggesting that most shrinkage was in fact appropriately controlled.

Dendritic organization

Figure 5 shows the distribution of cells along the CA3 to subiculum axis. There were no systematic variations noted in terms of overall morphology, except for variations in branching. In most of the cells the distinction between the basal and oblique (lateral branches in the apical dendrites) was quite well defined. One notable variability between cells is the point at which the apical dendrite bifurcates in the stratum radiatum. In general CA1 pyramidal cells demonstrated one to two apical dendrites, and in most cases the main apical stem bifurcated into two branches in the stratum radiatum, about 100 µm from the soma. In some neurons a single primary apical dendrite originated from the soma and then divided into two or more branches in the stratum lacunosum-moleculare. On average 45% of the in vitro cells and 20% of the in vivo cells showed an apical trunk bifurcation. Nearly all the basilar dendrites emerged from the base of the soma, coursed through the stratum oriens and terminated in the stratum oriens. Most oblique dendrites originating from the main apical trunk terminated entirely in the stratum radiatum. However, in five in vivo cells and one in vitro cell, there were a few dendrites that originated from the most proximal part of the apical trunk and coursed more like a basilar dendrite and terminated in the stratum oriens (Fig. 6A). In contrast, three in vivo cells showed dendrites that originated from one of the basilar tree branches and took a path more like an oblique branch and terminated in the stratum radiatum (Fig. 6B). There were two in vitro cells that demonstrated branches emerging from the lateral side of the soma, coursing their way through the cell layer and terminating in the region of the cell layer. For quantitative analysis we classified these lateral branches as part of the apical tree.

Dendrograms

Dendritic branching diagrams (dendrograms) of representative neurons are shown in Figure 7. The soma is not represented directly in the diagram but is located to the left of all the branching patterns of each neuron. The labels indicate the main dendrite originating from the soma as either apical (A1, A2, etc.) or basilar (B1, B2, etc.). The branching pattern is represented from left to right, starting with the main trunk or stem followed by branches emerging from subsequent divisions of the main trunk to the right. The dendrograms are to scale in terms of length and compared with each other, but dendritic diameters are not shown for clarity. The diagrams show the appropriate length of each branch segment and the pattern of the branch points. Dendritic complexity can be measured by branch order, which is incremented with each successive branch point, and can vary up to 25–30 for typical CA1 pyramidal cells (Table 1). Complexity includes both number of branches (which increases vertically), branch order (which increases horizontally), and length. There are large variations between neurons in terms of both branching and overall size of the dendritic trees, complementing the wide range of values for dendritic length (Fig. 7).

Summed geometric path length analysis

CA1 neurons from in vitro and in vivo preparations were evaluated using histograms of geometric (path) length between the soma and dendritic terminals. The geometric summated path length (Fig. 8) shows the distance along each possible path to individual dendritic terminal

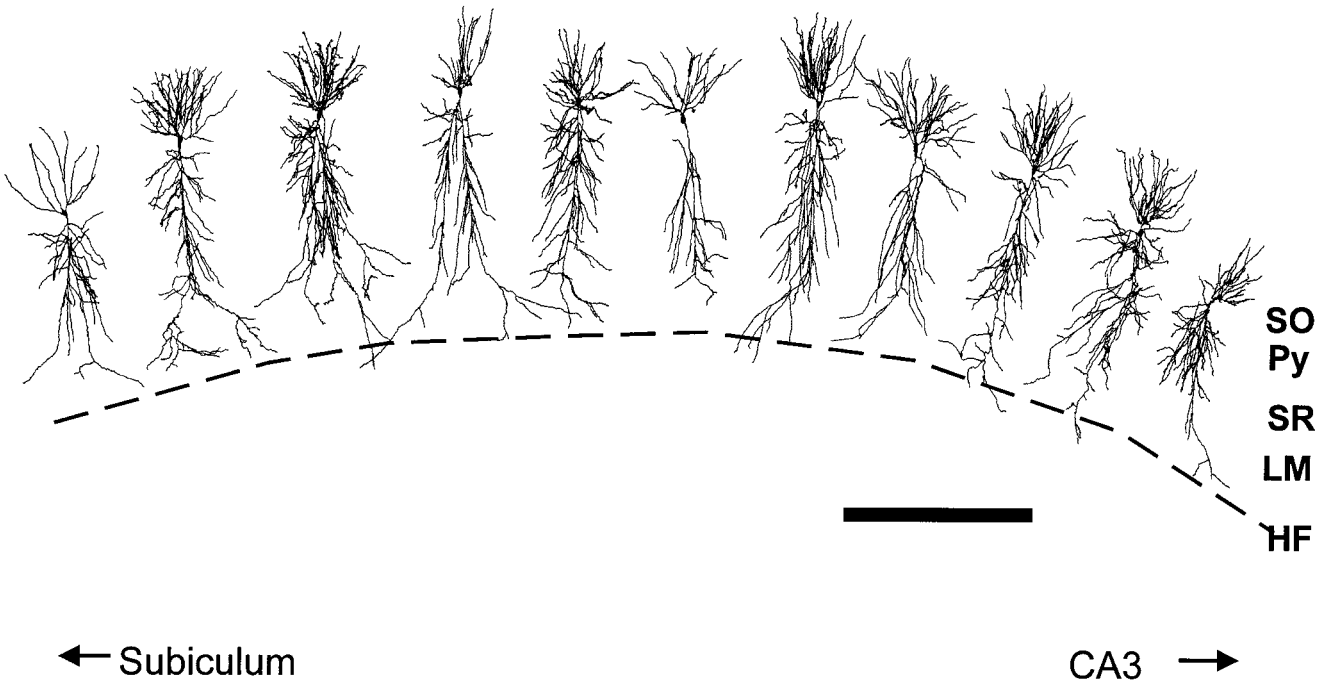

Fig. 5. A composite picture illustrating the organization of hippocampal CA1 pyramidal cells along the CA3 to subiculum axis. These are the computer-generated line drawings of CA1 cells labeled in vivo. Note the variable bifurcation of the primary apical dendrite within the stratum radiatum and the overall considerable branching differences between the cells. SO, stratum oriens; Py, stratum pyramidale; SR, stratum radiatum; LM, lacunosum-moleculare and HF, hippocampal fissure. Scale bar = 500 μm.

branches (one path is shown in bold as an example). This graph shows that additional branches primarily in the proximal stratum radiatum are present in the in vivo neurons. The overall maximum path length of the apical dendritic tree for the in vitro and in vivo cells was 700 and 800 μm, respectively. Most of the branches in the apical tree occurred between 100 and 400 μm from the soma in both groups. From this perspective the neurons showed considerable underlying similarity except for various minor differences in terms of branching structure.

Branch order length and density

Branch order analysis followed a centrifugal pattern, with branch order of 0 at the soma and incremented with each progressive branch point from the soma, toward the apical and basilar tips (Uylings et al., 1986). This analysis indicated that the highest branch order attained by the basilar tree was 15, whereas the apical tree showed considerably more complexity, to a branch order of 30; these values were not different for cells between the two groups (Fig. 9). The in vivo cells showed slightly more branches in the distal branch orders (five to nine) of the basilar trees. However, there was no difference in the number of branches in the apical tree between the groups (Fig. 9A). The length per branch order was similar throughout both apical and basilar dendritic trees for the in vitro and in vivo cells (Fig. 9B). Remarkably, there is no relationship between the branch order and the length of branches per branch order, suggesting that this value is a relative constant. Thus, for both groups of cells the CA1 pyramidal neurons show a high degree of branch complexity in both the apical and basilar trees, and a constant length of dendrite per branch order.

Electrotonic modeling

The goal of the modeling was to calculate an approximate passive electrical representation of the dendrites in the various subgroups of CA1 cells and to illustrate the dendritic processing of signals similar to those generated by synapses. Calculations were performed using a finite cable model representation and the detailed reconstruction data (Turner, 1984a, 1984b; Turner et al., 1991). Mean electrotonic distance or path length from the soma to all terminals (calculated from the dendritic structure using a constant specific membrane resistance of 30 $K\Omega$-cm^2) was similar in the two groups of neurons (Table 2). Figure 10 shows a graph of electrical distance of separated apical (to the right) and basilar (to the left) dendrites. Table 2 indicates that there was a difference in predicted input resistance values between the in vitro and in vivo neurons, primarily for the cylindrical cells. The predicted number of spines is also different, because the spine density follows a pattern related to dendritic length (Turner, 1984a), and may be an underestimate of the true number present. These electrotonic values imply that the bulk of the dendritic surface is close to the soma (within 1λ), although significant electrotonic waveform shaping and decreased synaptic peak height would be expected even for this short overall distance (see below; Turner, 1984b; Turner et al., 1991; Claiborne et al., 1992; Spruston et al., 1993, 1994). However, the functional or electrotonic analysis implies that the two different sets of CA1 pyramidal neurons with complex dendrites may be operating similarly.

Voltage transfer and synaptic efficacy

Because electrotonic length gives only a partial view of synaptic efficacy simulations were performed using both in

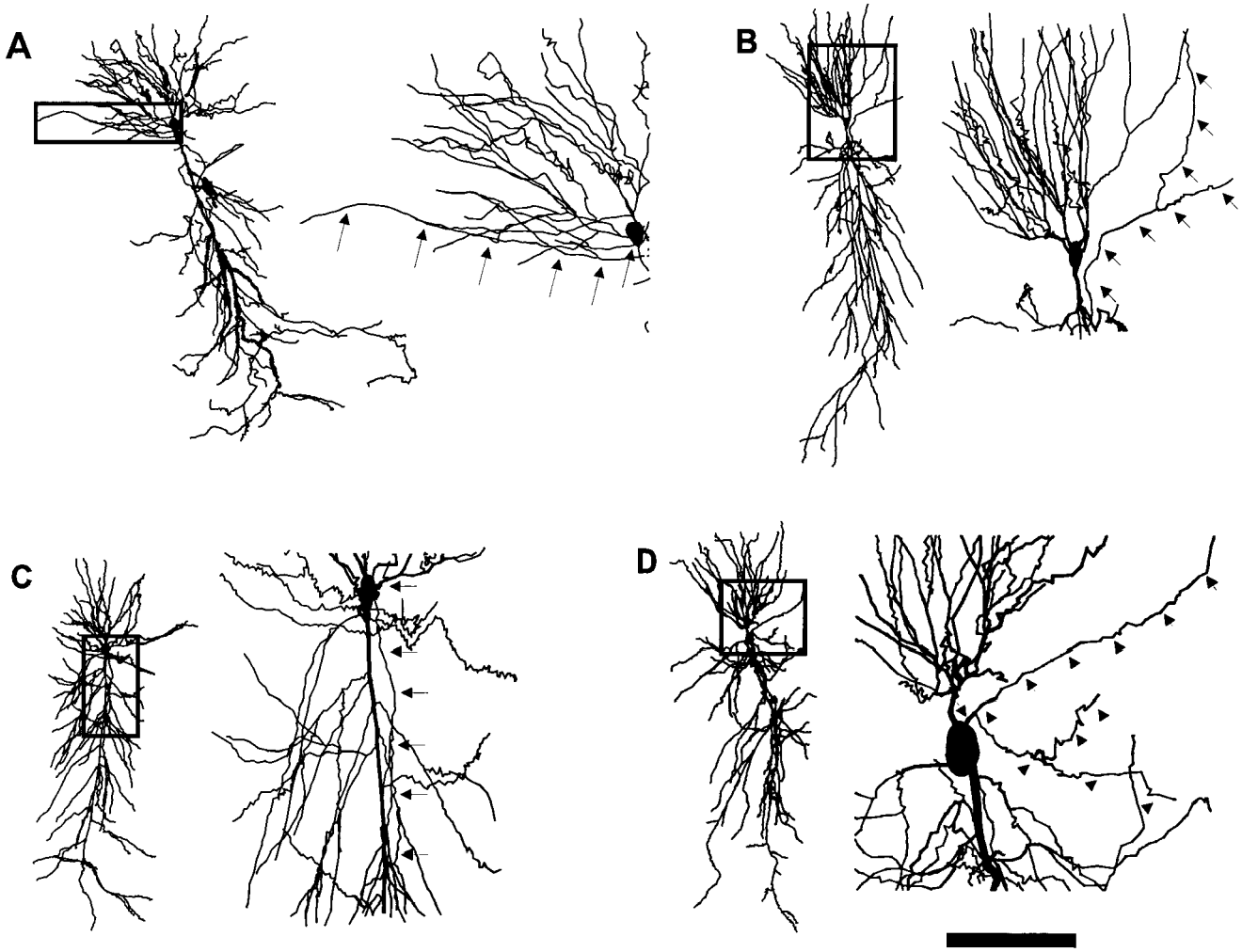

Fig. 6. Variations of dendritic tree origination in the CA1 pyramidal cells. **A,B:** Examples of cells in which apical oblique dendrites emerged from an initial apical dendritic branch but then coursed across the pyramidal cell layer and terminated in the stratum oriens, similar to a basilar dendrite. The boxed areas in A and B are detailed to the right, with the arrows denoting the branch that crosses the stratum pyramidale to functionally become a basilar dendritic branch. **C,D:** Cells with dendrites originating in the basilar tree but coursing across the pyramidal cell layer and terminating in the stratum radiatum, acting functionally as apical dendrites. The boxes show the regions of the detailed views to the right, in which arrows point out the branch crossing the stratum pyramidale. Scale bar = 200 μm in full-size views A–D, 87 μm in magnified view A, 63 μm in magnified view B, 38 μm in magnified view C, 46 μm in magnified view D.

vitro and in vivo cell types, to compare both orthograde (dendrite to soma) and retrograde (soma to dendrite) voltage transfer for two different typical signals. This analysis provides both an example of results for these reconstructed cells and also a functional comparison of the in vitro and in vivo cells. Multiple sites from each neuron (n = 24 dendritic sites from each cell, at varying electrotonic lengths from the soma) were randomly selected and the voltage transfer calculated using a passive cable model, as previously described (Turner, 1984b). There is a considerable difference in transfer in the two different directions (soma to dendrite and dendrite to soma). This direction-dependent passive conduction stems from the branching and terminations of the two pathways: the dendrite to soma pathway has a large somatic conductance, whereas the soma to dendrite path has a very small distal conductance, so less signal is attenuated in this direction. This typical result underscores the importance of dendritic branching considerations in signal attenuation in dendritic trees, as discussed in more detail in several current reports (Claiborne et al., 1992; Spruston et al., 1993, 1994; Mainen et al., 1996; Yuste and Tank, 1996).

Transient signals are attenuated much more heavily by cable structures than steady-state signals, as demonstrated by fast EPSP (non-NMDA) simulated synaptic potentials (Fig. 11B,D [using an $\alpha = 20$ and amplitude of 1.0 nS conductance change]). The voltage transfer from dendritic loci to the soma in both cell groups as a function of either steady-state or fast PSP (non-NMDA) inputs ($\alpha = 20$) is shown in Figure 11C,D. Note that most dendritic sites fall far below 50% signal transfer for the steady-state condition and the attenuation is even more significant for the simulated fast PSP (non-NMDA) synaptic inputs and the simulated action potentials. Figure 11A,B shows data for multiple sites but for signals conducted from the soma to dendritic sites. Even for the steady-state condition, there is only a moderate conduction from the soma to dendritic sites, although many sites show greater than

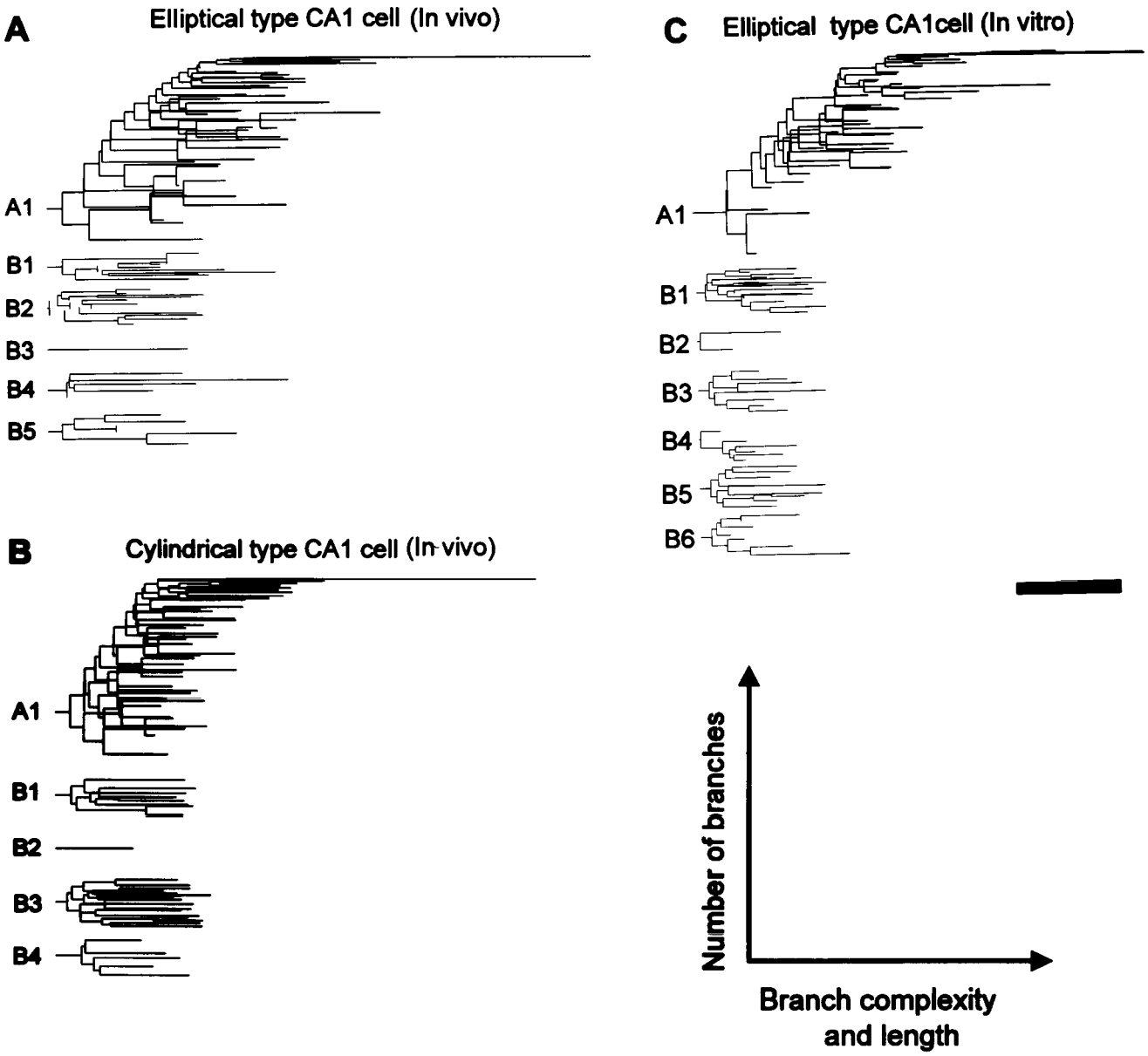

Fig. 7. Dendritic branching diagrams (dendrograms) of representative in vivo elliptical (**A**), in vivo cylindrical (**B**), and in vitro elliptical (**C**) cells. The soma is not shown in the diagrams but is located to the left of each cell. The labels indicate whether each main dendrite (originating at the soma) is an apical (A1, A2, etc.) or basilar branch (B1, B2, etc.), and the dendrite number. These diagrams show the general branching patterns of the apical and basilar dendritic tree for each representative cell. The dendrograms are to scale in terms of length and complexity, but dendritic diameters are not shown for clarity. The branching pattern is represented from left to right, starting with the main trunk or stem of the major dendrites followed by branches emerging from subsequent divisions of this main trunk, toward the right. Increasing branch order complexity is shown from left to right and number of branches is shown vertically. Scale bar = 200 μm.

50% transfer. The fast EPSP signal (passive) shows progressively more conduction loss. Thus, again despite a "short" electrotonic length, signal transfer in both directions between dendritic sites and the soma is severely attenuated. Overall, there was very little difference in the degree of signal attenuation between the two groups of neurons, suggesting similar principles of electrotonic organization.

DISCUSSION

We quantified the three-dimensional morphology of CA1 pyramidal cells from two different sources and eliminated an important bias inherent in comparing data from different laboratories by performing an identical form of computer-based reconstruction on neurons labeled in vitro and in vivo. The findings indicate that CA1 pyramidal cells in the intact brain are quite uniform, independent of their subiculofimbrial position and possess a cylindrical shape, similar to CA3 pyramidal cells (Turner et al., 1995). Our measures of dendritic lengths and number of segments of neurons reconstructed from in vitro slices are in good agreement with previous studies, including the observed cylindrical or elliptical shape (Amaral et al., 1990; Pyapali and Turner, 1994, 1996; Bannister and Larkman, 1995;

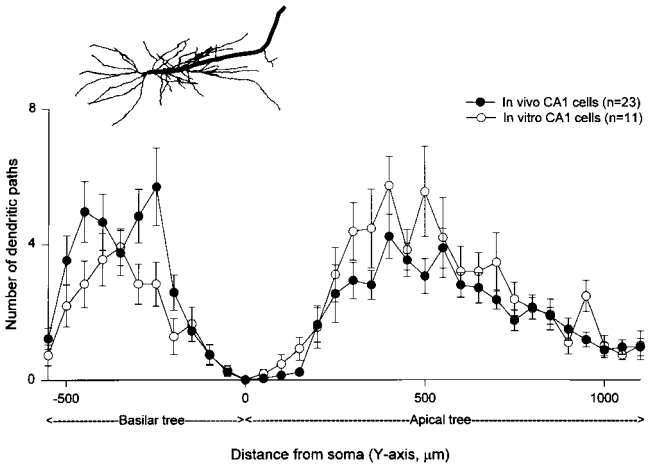

Fig. 8. A histogram of summated dendritic path lengths to all terminals, from the soma. The inset diagram shows a cell with a path length in bold. There was no difference in the number of dendritic terminals between the in vitro and in vivo neurons.

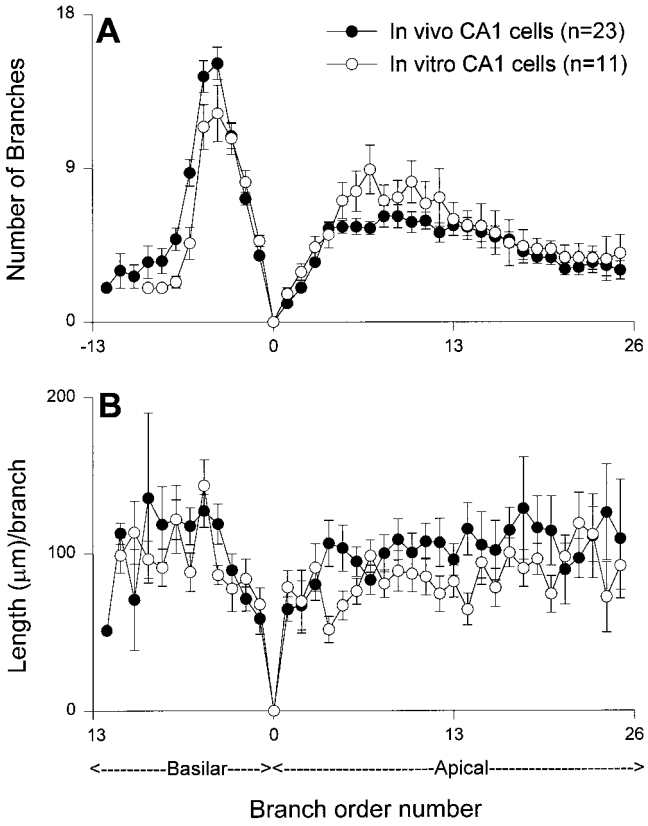

Fig. 9. Branch order analyses for the number of branches (**A**) and the average dendritic length per branch (**B**) at each order clearly shows no difference between or among the groups. Basal dendrites are represented to the left and apical dendrites are to the right. The branch order was evaluated in a centrifugal fashion, with the first branch order being the most dendrites attached to the soma. The branch order value then incremented at each branch point. The length of branches does not appear to change substantially as a function of branch order, even though it varies between the two groups. Values represent mean ± SEM.

TABLE 2. Cell Electrical Parameters—CA1 Cells[1]

Parameter	In Vitro (n = 11)	In Vivo (n = 23)	*P* Value
Constant R_m = 30 KΩ-cm² and R_i = 200 Ω-cm			
Predicted R_N (MΩ)	45.8 ± 20.8	59.2 ± 28.1 NS	
Mean terminal X (λ)	0.75 ± 0.28	0.77 ± 0.16 NS	
Predicted spines (×10³)	23.9 ± 7.46	25.7 ± 6.20 NS	
Elliptical cells		*P* value a vs b	*P* value a vs c
Predicted R_N (MΩ)	56.1 ± 23.1[a]	47.7 ± 19.0[b]NS	NS
Mean terminal X (λ)	0.83 ± 0.38[a]	0.79 ± 0.13[b]NS	NS
Predicted spines (×10³)	21.0 ± 4.89[a]	28.4 ± 5.39[b]**	NS
Cylindrical cells		*P* value c vs d	*P* value b vs d
Predicted R_N (MΩ)	37.2 ± 15.6[c]	77.3 ± 31.3[d]**	**
Mean terminal X (λ)	0.68 ± 0.16[c]	0.74 ± 0.21[d]NS	NS
Predicted spines (×10³)	25.9 ± 8.11[c]	21.8 ± 4.84[d]NS	**

[1]R_N is the input resistance at the soma of each neuron, R_i is the specific internal resistivity and R_m is the specific membrane resistivity. The estimated electrotonic values were calculated using these assumptions and a "standard" spine density formula, with the resulting predicted number of spines. NS implies that the values are not significantly different; single asterisk implies $P < 0.05$; double asterisk implies $P < 0.01$ (see text for a description of the statistical tests).

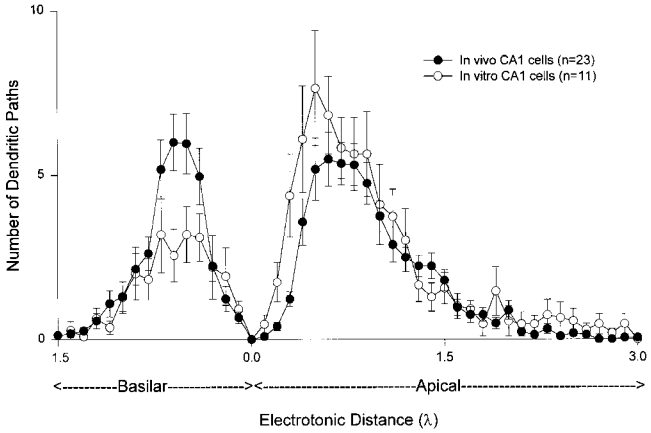

Fig. 10. Plot of electrotonic distance from the soma to dendritic terminations along all possible path lengths throughout the dendrites, comparing the two cell groups. This plot shows the summated length from the soma to each terminal, as measured in the individual electrotonic lengths of each segment along the path. This graph was comparable to the geometric length plot (Fig. 8) and reflects no difference in the two groups of neurons. Note that most of the terminations end at less than 1.0λ, suggesting an electrical compactness.

Ishizuka et al., 1995). Dendritic trees of CA1 pyramidal cells appear to be among the most complex in the brain in terms of branching complexity. Our modeling data suggest that the passive cable properties of dendritic branches lead to a significant attenuation of synaptic signals propagating from dendritic sites to the soma. These functional aspects are similar for both in vitro and in vivo neurons, indicating a common underlying organization of these dendritic properties from two different sources.

Comparison between in vivo and in vitro labeled neurons

The total dendritic lengths of the in vivo labeled CA1 pyramidal cells were consistently similar to their in vitro labeled counterparts, after adequate correction for shrinkage. However, size differences between in vivo and in vivo neurons have been observed for CA3 pyramidal cells (Turner et al., 1995). Furthermore, most in vivo labeled CA1 pyramidal cells possessed similar dendritic extent in

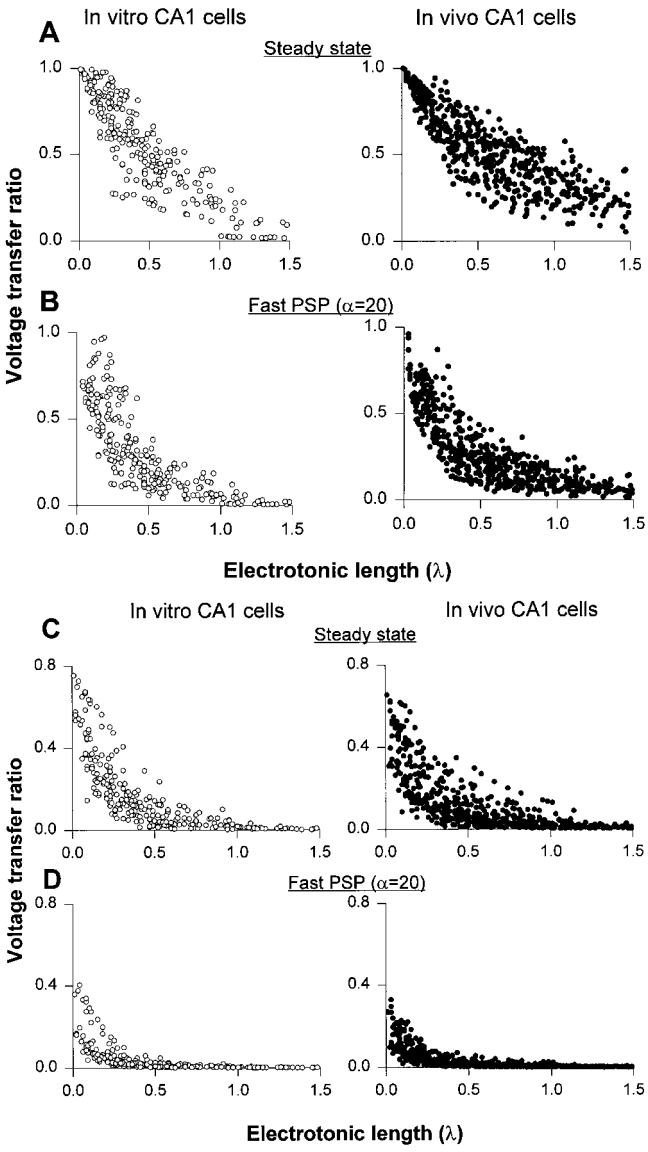

Fig. 11. Signal conduction from soma to dendrite (**A,B**) and from dendrite to soma (**C,D**) for representative dendritic sites on all CA1 cells labeled in vitro (left) and in vivo (right). Orthodromic voltage transfer values from these individual dendritic sites to the soma are plotted vs. electrotonic distance to that dendritic site. The vertical scatter of individual values indicates the range of transfer values for different sites that possess the same electrotonic length. The conduction from dendrite to soma shows much less transfer for fast postsynaptic potentials (PSPs) than steady-state signals. Most sites show less than 5% voltage transfer to the soma for even the fast PSP signal, despite the relatively short electrotonic length. Retrograde voltage transfer was plotted vs. electrotonic distance to that dendritic site. The vertical scatter of individual values indicates the range of transfer values for different sites that possess the same electrotonic length. Although retrograde voltage transfer is much greater than orthograde transfer there is still considerable loss for most sites, with less than half the sites showing even 50% voltage transfer with the steady-state somatic input.

the X-Y and Y-Z directions (i.e., the dendritic tree was cylindrical), whereas the extent of the dendritic arbor was more truncated in the Y-Z than in the X-Y axis for the in vitro neurons (a more elliptical appearance), but became similar after adequate correction for shrinkage. Several additional factors may contribute to similarities and differences between these groups of neurons, including technical sources or a sampling bias. Although animals used for in vivo recordings were slightly larger (200–500 gram) than those used in vitro (180–200 gram), the alveus-to-hippocampal fissure distance was similar in the two groups. Strain differences (Sprague-Dawley in vivo vs. Fischer 344 in vitro) may be another contributing factor. However, the quantitative data and the elliptical appearance of the neurons in our in vitro experiments are very similar to those previously labeled cells in vitro in different rat strains (Amaral et al., 1990; Pyapali and Turner, 1994, 1996; Bannister and Larkman, 1995; Ishizuka et al., 1995).

The degree of shrinkage was similar between the in vitro and in vivo neuron groups, for similar types of processing, particularly the light microscopic protocol. However, there was considerably heightened depth shrinkage using this protocol, due primarily to the dehydration step and air drying, as shown by measurements before and after this step. The shrinkage with the light microscopic processing was consistent (10–11% in the X and Y axes and 75% in the depth) across several different types of measurements in several laboratories. This shrinkage is considerably more than previous studies that did not use dehydration but rather 100% glycerol for clearing (Ishizuka et al., 1995; Turner and Schwartzkroin, 1980), in which case the entire shrinkage was less than 10% in each axis. Other studies have measured shrinkage in different ways, for example Trommald et al. (1995) measured the shrinkage of individual neuronal processes rather than the tissue, resulting in 20% shrinkage in each of the X and Y planes and 41% shrinkage in the depth, after a different fixative protocol and dehydration processing. Other studies have mentioned shrinkage but have not shown any systematic measurements, particularly Golgi studies indicating at least 20–30% shrinkage in the X and Y dimensions but depth shrinkage is not commonly mentioned (Uylings et al., 1986). Our current measurements are similar to previous estimates for CA3 neurons as well (Turner et al., 1995). An additional method to decrease shrinkage is to use the electron microscopic protocol for processing, including cryoprotection and osmification as well as Durcupan embedding, applied to several of our neurons in this study, which showed considerably reduced depth shrinkage presumably due to the stiffness of the substrate.

In principle, it is possible that the brain slicing technique may limit the size of the neurons (particularly in the septotemporal direction or the depth of the slice) due to necrosis of the edges of the slices to less than 200 μm, leading to the inadvertent selection bias toward small, elliptical neurons. Several arguments can be made against this possibility, however. First, in vivo cells processed for light microscopy had a strong overlap with the in vitro labeled cells, suggesting that shrinkage in the Z dimension was a significant factor. Second, when the brain was cut parallel with the longitudinal axis of the hippocampus, the axes of the elliptical dendrites were reversed and their Y Z extent was similar to the X Y extent of neurons derived from coronal sections. Third, all neurons embedded in Durcupan to prevent shrinkage after histologic staining had a cylindrical appearance. Thus, the morphometric similarities after correction for shrinkage imply that the CA1 pyramidal neurons arise from likely a similar under-

lying population of cells. Overall, our findings indicate that different recording and embedding conditions can significantly affect conclusions regarding both the morphometric and shape aspects of the dendritic tree, unless adequate correction is made for shrinkage. Our findings indicate that CA1 pyramidal cells in the intact brain likely uniformly possess a cylindrical shape.

Anatomical characteristics of CA1 pyramidal neurons

Qualitatively, CA1 pyramidal cells filled in vivo and in vitro demonstrated similar dendritic characteristics. The characteristics include the clear separation of dendritic branching patterns in each stratum, the small soma size and the predominance of a single major apical trunk dendrite. Dendritic branching patterns specific to CA1 pyramidal neurons include the large number of transverse branches off the single or double apical dendrite in the stratum radiatum, the peculiar manner in which only a few major apical branches penetrate into the stratum lacunosum-moleculare before branching adjacent to the hippocampal fissure and the large breadth of these branches along the hippocampal fissure. With these characteristics in mind, CA1 pyramidal cells showed a remarkable homogeneity, with the primary difference being the location of the bifurcation of the main apical trunk if it occurs. However, in agreement with an earlier report (Bannister and Larkman, 1995), we did not notice any difference between the cells with and without the bifurcation for the various groups of cells. In our sample, we did not have any cells with more than two major apical dendrites, unlike an earlier report (Turner and Schwartzkroin, 1980). However, this early report using horseradish peroxidase labeling may have shown multiple cell fills that were difficult to discriminate into individual neurons.

Several qualitative and quantitative differences between CA1 and CA3 pyramidal cells, labeled in vivo and reconstructed by the same tracing method, can be pointed out (Turner et al., 1995). The CA3 pyramidal neurons from the CA3a regions are larger than the CA1 neurons in terms of soma size and dendritic length. CA3 pyramidal neurons typically show vertical branching within the stratum radiatum, with a clear area in the distal stratum radiatum for the location of the Schaffer collateral bundle coursing toward CA1 (Ishizuka et al., 1995). Additionally, the CA3 neurons show much less extensive branching, with only 8–12 branch orders, whereas the CA1 neurons show up to 25–30 branch orders and are much more complex in structure. Many more of the CA3 apical dendritic branches penetrate into the stratum lacunosum-moleculare, whereas these branches show only minimal subbranches at this level. However, CA1 pyramidal neurons show only two to three apical branches perforating into the stratum lacunosum-moleculare, but these branches then show extensive further branching and traverse along the hippocampal fissure extensively. The volume occupied by CA3 pyramidal cells is larger but their total dendritic lengths are comparable with CA1 cells (18.1 vs. 17.4 mm). It must be pointed out, however, that these comparisons of average parameters do not reveal the often large individual differences between neurons.

Dendritic branches are densely covered with spines. Although spine density measurements were not directly carried out on these neurons, the surface increase by the addition of spines was approximated by using previously published data in the modeling studies (Turner, 1984a; Trommald et al., 1995). During development, the distance within the stratum radiatum and from the alveus to the hippocampal fissure gradually increases, although the cell's processes are likely always anchored at each end, between the ventricular surface and the pia at the fissure (Minkwitz and Holz, 1975; Minkwitz, 1976; Pokorny and Yamamoto, 1981). Therefore, the overall extent of these cells increases both by this overall Y axis extent increase with development and maturation and also by adding side branches within each layer, which may be influenced by the types and number of synaptic inputs each neuron receives (Ishizuka et al., 1995). This view of ontogenesis of pyramidal cell dendrites suggests that the basic structure and orientation of the main dendrites is predetermined early in development by the anchorage of the apical and basilar terminations, but the presence and/or addition of small branches is determined by later functional activity and synaptic innervation patterns. With both denervation and aging, dendritic form and function are altered, suggestive of dendritic remodeling (Pyapali and Turner, 1994, 1996). Because CA1 pyramidal neurons maintain a very plastic form of (low molecular weight) neurofilaments, active dendritic remodeling may actually be the usual state, with responses to denervation and other stresses rapidly appearing. This possibility is in contrast to CA3 pyramidal neurons, which possess much more stable neurofilaments, which are considered developmentally more mature (Shetty and Turner, 1995).

Functional characteristics of CA1 pyramidal neurons

CA1 neurons labeled in vivo and in vitro seem to be morphologically and electrically similar, indicating an underlying commonality of synaptic integration and signal processing of these neurons. CA1 pyramidal cells possess complex dendritic morphology and a large complement of synaptic inputs and ligand-gated receptors, together with multiple voltage-dependent conductances (Turner et al., 1991; Spruston et al., 1993, 1995; Christie et al., 1995; Yuste and Tank, 1996; Magee and Johnston, 1997; Stuart et al., 1997). Our passive modeling highlights only one initial and basic aspect of this complex functioning, but which provides the framework for additional properties and also demonstrates some basic results for comparison with more complex studies. Although the histogram of electrotonic distance paths to terminals suggests that overall CA1 pyramidal cell dendrites are electrically compact, electrotonic distance alone does not directly point to signal propagation characteristics. The nonlinear characteristics of dendrites may significantly and transiently alter the functional capabilities of neurons and thus will likely prove to be highly interested as these can be further studied using both predictive modeling and physiologic methods.

However, as previously described by Andersen et al. (1980), simultaneous activation of only a few hundred excitatory synapses (out of greater than 40,000 to 60,000; Li et al., 1994), each contributing a small voltage input, is required for cell discharge. Thus, because of the small size of the somatic potential contributed by each synaptic input and the large attenuation in the dendrite to soma direction, at least 1% of the excitatory inputs must arrive synchronously to activate a CA1 pyramidal cell with passive dendritic properties only. In vivo, these postsynap-

tic neurons can be modulated by a large number of additional sources, including various forms of inhibition, monoaminergic, serotoninergic, and cholinergic synapses, as well as intrinsic signaling proteins within each neuron. Because CA3 neurons communicate with their CA1 pyramidal cell partners via only a few (typically only one) synapse (Malinow, 1991; Sorra and Harris, 1993; Li et al., 1994), the above physiologic observations support the considerable potential importance of active dendritic mechanisms for the amplification of synaptic inputs (for reviews, see Spruston et al., 1994; Yuste and Tank, 1996).

The similarities between the in vitro and in vivo labeled neurons are also shown by the responses to inputs at the dendritic and somatic levels, which are determined by factors such as branching rather than solely by electrotonic length. The passive signal propagation capabilities of these neurons are significantly limited by a high degree of attenuation for both steady-state and transient inputs, due to the branching characteristics and high numbers of branch orders. This significant degree of attenuation, despite relatively short electrotonic lengths to dendritic terminations, emphasizes that electrotonic length alone does not define the degree of signal propagation. Thus, "electrically short" dendritic trees may lead to considerable signal attenuation, particularly in complex trees such as observed in these CA1 pyramidal neurons. Many of these aspects of signal propagation are moderated and enhanced by voltage-dependent and ligand-gated channel properties and thus the passive framework described here remains only an initial description of dendritic function, to be superseded by more complex and realistic dendritic models as they become available. These models are currently limited by lack of knowledge regarding the detailed dendritic and spatial distribution of ligand-gated receptors and conductances, although simulated synaptic inputs are well modeled by an α function (Turner, 1984a, 1984b).

Although beyond the modeling presented here, additional interesting characteristics of CA1 pyramidal neurons include a diffuse distribution of voltage-dependent sodium channels, calcium channels, and potassium channel, although the density of distribution is unknown. The passive data simulating an action potential suggest that passive conduction alone of a signal as fast as an action potential is highly insecure in these dendrites, in either direction (Buzsaki et al., 1996). Even back-propagation of an action potential will clearly require an adequate density of sodium channels, and forward or orthograde propagation would require a much higher density due to effect of a small current in a side branch being diluted as it enters a larger, more proximal branch. How far orthodromic and retrograde action potentials are propagated remains a large question, although a sufficient density of sodium channels is likely present for at least an isolated action potential in more distal dendritic regions. Action potential conduction from soma to dendritic sites may depend critically on the conduction path and whether other conductances are activated, particularly inhibitory conductances. Such inhibitory events may function as a shunt, preventing voltages from passing either way on the path, selectively tuning information available to the soma as a function of overall inhibition. Thus, starting from the passive properties described here more complex inferences may be envisioned, although additional compartmental modeling may be a more appropriate avenue in which to adequately address these issues. However, the reconstructed cells described here are freely available in Neurolucida format for such additional modeling, using the structure as a starting point.

ACKNOWLEDGMENTS

This research was supported by National Institutes of Health grants (NS-29482 and AG-13165) to D.A.T., (NS-27058, NS-28121, and NS-02383) to G.B., and (5T32 AG-00029-17) to G.K.P.; by Human Frontier Science Foundation funds to G.B.; by Whitehall Foundation funds to G.B.; and by a Veterans Affairs Medical Center Merit Review Award to D.A.T. Please contact D.A. Turner (turne008@mc.duke.edu) for further information regarding dissemination of the digitized cell data and available data formats of these cells.

LITERATURE CITED

Amaral, D.G, N. Ishizuka, and B. Claiborne (1990) Neurons, numbers and the hippocampal network. Prog. Brain Res. *83:*1–9.

Andersen, P., H. Silfvenius, S.H. Sundberg, and O. Sveen (1980) A comparison of distal and proximal dendritic synapses on CA1 pyramids in guinea-pig hippocampal slices in vitro. J. Physiol. (Lond.) *307:*273–299.

Bannister, N.J., and A.U. Larkman (1995) Dendritic morphology of CA1 pyramidal neurons from the rat hippocampus: 1. Branching patterns. J. Comp. Neurol. *360:*150–160.

Blackstad, T.W. (1985) Laminar specificity of dendritic morphology: Examples from guinea pig hippocampal region. In L.F. Agnati, and K. Fuxe (eds): Quantitative Neuroanatomy in Transmitter Research. London: MacMillan, pp. 55–69.

Buckmaster, P.S., and P.A. Schwartzkroin (1995) Physiological and morphological heterogeneity of dentate gyrus-hilus interneurons in the gerbil hippocampal in vivo. Eur. J. Neurosci. *7:*1393–1402.

Buzsaki, G., M. Penttonen, Z. Nadasdy, and A. Bragin (1996) Pattern and inhibition-dependent invasion of pyramidal cell dendrites by fast spikes in the hippocampus in vivo. Proc. Natl. Acad. Sci. USA *93:*9921–9925.

Christie, B.R., L.S. Eliot, K. Ito, H. Miyakawa, and D. Johnston (1995) Different Ca2+ channels in soma and dendrites of hippocampal pyramidal neurons mediate spike-induced Ca2+ influx. J. Neurophysiol. *73:*2553–2557.

Claiborne, B.J., A.M. Zabor, Z.F. Mainen, and T.H. Brown (1992) Computational models of hippocampal neurons. In T. McKenna, J., Davis, S.F., Zornetzer (eds): Single Neuron Computation. New York: Academic Press, Inc., pp. 61–80.

Henze, D.A., W.E. Cameron, and G. Barrionuevo (1996) Dendritic morphology and its effects on the amplitude and rise-time of synaptic signals in hippocampal CA3 pyramidal cells. J. Comp. Neurol. *369:*331–344.

Ishizuka, N., W.M. Cowan, and D.G. Amaral (1995) A quantitative analysis of the dendritic organization of the pyramidal cells in the rat hippocampus. J. Comp. Neurol. *362:*17–45.

Li, X.G., P. Somogyi, A. Ylinen, and G. Buzsaki (1994) The hippocampal CA3 network: An in vivo intracellular labeling study. J. Comp. Neurol. *339:*181–208.

Lingenhohl, K., and D.M. Finch (1991) Morphological characterization of entorhinal neurons in vivo: Soma-dendritic structure and axonal domains. Exp. Brain Res. *84:*57–74.

Lipowsky, R., T. Gillessen, C. Alzheimer (1997) Dendritic Na+ channels amplify EPSPS in hippocampal CA1 pyramidal cells. J. Neurophysiol. *76:*2181–2191.

Lopez da Silva, F.H., M. Witter, P.H. Boeijiga, and A. Lohman (1990) Anatomical organization and physiology of the limbic cortex. Physiol. Rev. *70:*453–511.

Lorente de No, R. (1934) Studies on the structure of the cerebral cortex. II. Continuation of the study of the ammonic system. J. Psychol. Neurol. (Leipzig) *46:*113–157.

Magee, J.C., and D. Johnston (1997) A synaptically controlled, associative signal for Hebbian plasticity in hippocampal neurons. Science *275:* 209–13.

Mainen, Z.F., N.T. Carnevale, A.M. Zador, B.J. Claiborne, and T.H. Brown (1996) Electrotonic architecture of hippocampal CA1 pyramidal neu-

rons based on three-dimensional reconstructions. J. Neurophysiol. *76:*1904–1923.

Major, G., A.U. Larkman, P. Jonas, B. Sakmann, and J.J.B. Jack (1994) Detailed passive cable models of whole-cell recorded CA3 pyramidal neurons in rat hippocampal slices. J. Neurosci. *14:*4613–4638.

Malinow, R. (1991). Transmission between pairs of hippocampal slice neurons: Quantal levels, oscillations and LTP. Science *252:*722–724.

Migliore, M., E.P. Cook, D.B. Jaffe, D.A. Turner, and D. Johnston (1995) Computer simulations of morphologically reconstructed CA3 hippocampal neurons. J. Neurophysiol. *73:*1157–1168.

Minkwitz, H.G. (1976) Zur Entwicklung der Neuronenstruktur des Hippocampus wahrend der Pra- und Postnatalen Ontogenese der Albinoratte. III. Mitteilung: Morphometrische Erfassung der Ontogenetischen Veranderungen in Dendriten-Struktur und Spine Besatz an Pyramidanen-Neuronen (CA1) des Hippocampus. J. Hirnforsch. *17:*255–275.

Minkwitz, H.G., and L. Holz (1975) Die Ontogenetischentwicklung von Pyramiden neuronen aus dem Hippocampus (CA1) der Ratte. J. Hirnforsch. *16:*37–54.

Pokorny, J., and T. Yamamoto (1981) Postnatal ontogenesis of hippocampal CA1 area in rats: Development of dendritic arborization in pyramidal neurons. Brain Res. Bull. *7:*113–120.

Pyapali, G.K., M. Penttonen, A. Ylinen, G. Buzsaki, and D.A. Turner (1995) Comparative dendritic structure of rat CA1 pyramidal neurons labeled in vitro and in vivo. Neurosci. Abstr. *21:*597.

Pyapali, G.K., and D.A. Turner (1994) Denervation-induced alterations in CA1 pyramidal neurons following kainic acid lesions in rats. Brain Res. *652:*279–290.

Pyapali, G.K., and D.A. Turner (1996) Increased dendritic extent in hippocampal CA1 neurons from aged Fischer 344 rats. Neurobiol. Aging *17:*601–611.

Ramon y Cajal, S. (1911) Histologie du Systeme Nerveux de l'Homme et des Vertebres. Paris: Maloine.

Shetty, A.K., and D.A. Turner (1995) Non-phosphorylated neurofilament protein immunoreactivity in adult and developing rat hippocampus: Specificity and application in grafting studies. Brain Res. *676:*293–306.

Sik, A., A. Ylinen, M. Penttonnen, and G. Buzsaki (1994) Inhibitory CA1-CA3-hilar feedback in the hippocampus. Science *265:*1722–1724.

Sik, A., M. Penttonen, A. Ylinen, and G. Buzsaki (1995) Hippocampal CA1 interneurons: An in vivo intracellular labeling study. J. Neurosci. *15:*6651–6665.

Sorra, K.E., and K.M. Harris (1993) Occurrence and three-dimensional structure of multiple synapses between individual radiatum axons and their target pyramidal cells in hippocampal area CA1. J. Neurosci. *13:*3736–3748.

Spruston, N., and D. Johnston (1992) Perforated patch-clamp analysis of the passive membrane properties of three classes of hippocampal neurons. J. Neurophysiol. *67:*508–529.

Spruston, N., D.B. Jaffe, and D. Johnston (1994) Dendritic attenuation of synaptic potentials and currents: The role of passive membrane properties. TINS *17:*161–166.

Spruston, N., D.B. Jaffe, S.H. Williams, and D. Johnston (1993) Voltage and space-clamp errors associated with the measurement of electrotonically remote synaptic events. J. Neurophysiol. *70:*781–802.

Spruston, N., Y. Schiller, G. Stuart, and B. Sakmann (1995) Activity-dependent action potential invasion and calcium influx into hippocampal CA1 dendrites. Science *268:*297–300.

Stockley, E.W., H.M. Cole, A.D. Brown, and H.V. Wheal (1993) A system for quantitative morphological measurement and electrotonic modelling of neurons: Three-dimensional reconstruction. J. Neurosci. Methods *47:* 39–51.

Stuart, G., N. Spruston, B. Sakmann, and M. Hausser (1997) Action potential initiation and backpropagation in neurons of the mammalian CNS. TINS *20:*125–131.

Trommald, M., V. Jensen, and P. Andersen (1995) Analysis of dendritic spines in rat pyramidal cells intracellularly filled with a fluorescent dye. J. Comp. Neurol. *353:*26–274.

Turner, D.A. (1984a) Segmental cable evaluation of somatic transients in hippocampal neurons (CA1, CA3 and Dentate). Biophys. J. *46:*73–84.

Turner, D.A. (1984b) Conductance transients onto dendritic spines in a segmental cable model of CA1 and dentate hippocampal neurons. Biophys. J. *46:*85–96.

Turner, D.A., and P.A. Schwartzkroin (1980) Steady state electrotonic analysis of intracellularly-stained hippocampal neurons. J. Neurophysiol. *44:*184–199.

Turner, D.A., H.V. Wheal, E.W. Stockley, and H.M. Cole (1991) Three-dimensional reconstructions and analysis of the cable properties of neurons. In J. Chad and H.V. Wheal (eds): Cellular Neurobiology. Oxford: Oxford University Press, pp. 225–246.

Turner, D.A., X.G. Li, G.K. Pyapali, A. Ylinen, and G. Buzsaki (1995) Morphometric and electrical properties of reconstructed hippocampal CA3 neurons recorded in vivo. J. Comp. Neurol. *386:*580–595.

Uylings, H.B.M, A. Ruiz-Marcos, and J.V. Pelt (1986) The metric analysis of three-dimensional dendritic tree patterns: A methodological review. J. Neurosci. Methods *18:*127–151.

van den Pol, A.N., and F. Gallyas (1990) Trauma-induced Golgi-like staining of neurons: A new approach to neuronal organization and response to injury. J. Comp. Neurol. *296:*654–673.

Yuste, R., and D.W. Tank (1996) Dendritic integration in mammalian neurons, a century after Cajal. Neuron *16:*701–716.